Ecotoxicology and Environmental Safety 306 (2025) 119285

Contents lists available at ScienceDirect

Ecotoxicology and Environmental Safety

journal homepage: www.elsevier.com/locate/ecoenv

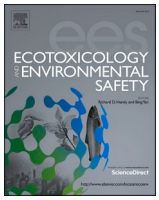

Low-dose polystyrene microplastics exposure promotes human prostate cancer cell proliferation via GPX4-mediated ferroptosis

Jingmo Li [a,1], Chenyao Deng [b,1], Wenyu Zou [c,1], Xindi Jiang [a], Yinuo Dong [a], Zidi Yan [a], Hui Jiang [b,*], Jia Zheng [a,c,**], Zirun Jin [a,b,**]

[a] Research Center, Peking University First Hospital, Beijing 100034, China
[b] Department of Urology, Peking University First Hospital; The Institution of Urology, Peking University; Beijing Key Laboratory of Urogenital Diseases (Male) Molecular Diagnosis and Treatment Center; National Urological Cancer Center, Beijing 100034, China
[c] Department of Endocrinology, Peking University First Hospital, Beijing 100034, China

ARTICLE INFO

Edited by Tao Zhang

Keywords:
Polystyrene microplastic
Prostate cancer
Proliferation
GPX4
Ferroptosis

ABSTRACT

Microplastics are increasingly recognized as potential threats to human health. In our previous study, polystyrene microplastics (PS-MPs) were detected in both para-tumor and tumor tissues of human prostate samples, with significantly higher abundance observed in tumor tissues compared to their paired para-tumor counterparts. However, whether and how PS-MPs contribute to the progression of prostate cancer remains poorly understood. This study aims to investigate the effects and underlying mechanisms of PS-MPs exposure on the proliferation of human prostate cancer cells. To this end, we exposed both the human prostate cancer cell line LNCaP and primary cultured human prostate cancer cells to varying doses of 1-μm-diameter PS-MPs. Our results showed that low-dose (0.1 μg/mL) PS-MPs exposure for 48 significantly promoted the proliferation of LNCaP cells. Additionally, PS-MPs exposure altered the expression of certain inflammatory factors and induced oxidative stress in LNCaP cells. We also observed upregulation of GPX4 and ACSL4 in LNCaP cells and primary prostate cancer cells following PS-MPs exposure. Notably, GPX4 knockdown reversed the effects of PS-MPs on reactive oxygen species (ROS) levels, lipid peroxidation, and glutathione content, likely by promoting ferroptosis. Taken together, our findings highlight a critical role for ferroptosis in PS-MPs-induced proliferation of human prostate cancer cells under low-dose exposure.

1. Introduction

Prostate cancer, one of the most common malignant tumors of the genitourinary system, is a major contributor to rising mortality among men worldwide (Sekhoacha et al., 2022; Gandaglia et al., 2021; Center et al., 2012). It presents with symptoms such as difficulty in urination, hematuria, and bone pain, which significantly impair patients' quality of life (Almeeri et al., 2024; Hansen et al., 2023). Projections indicate that the incidence of prostate cancer in China will increase dramatically, rising from the seventh to the third most common malignancy between 2015 and 2030 (Sung et al., 2021; Shi et al., 2022). Established risk factors of prostate cancer include genetic predisposition, hormonal imbalances, lifestyle factors, and environmental pollution (Bergengren et al., 2023; Perdana et al., 2016).

In modern society, microplastic pollution-resulting from the extensive use of plastic products and its potential threat to human health have attracted widespread attention (Thompson et al., 2024; Chartres et al., 2024). Microplastics, recognized as one of the major emerging health hazards, can enter the human body through ingestion, inhalation, and dermal absorption, and may accumulate in organs such as the lungs, gastrointestinal tract, and liver (Hunt et al., 2024; Liu et al., 2023). Once internalized, they have been shown to disrupt redox balance, alter endocrine hormones, interfere with cell cycle regulation, and trigger inflammatory responses, potentially contributing to a range of diseases including male reproductive disorders and the progression of cancer (Goswami et al., 2024; Prado et al., 2023; Fu et al., 2024).

Microplastics have been identified in human testes, semen, prostate gland and even prostate cancer tissues (Demirelli et al., 2024; Deng

* Corresponding author.
** Corresponding authors at: Research Center, Peking University First Hospital, Beijing 100034, China.
E-mail addresses: jianghui@bjmu.edu.cn (H. Jiang), zhengjia@bjmu.edu.cn (J. Zheng), jinzirun@bjmu.edu.cn (Z. Jin).
[1] These authors contributed equally to this work.

https://doi.org/10.1016/j.ecoenv.2025.119285
Received 14 August 2025; Received in revised form 11 October 2025; Accepted 21 October 2025
Available online 27 October 2025

et al., 2024). Studies have reported the presence of various plastic particles, such as polystyrene, polyamides, polyglycol terephthalate, and polyvinyl chloride, in para-tumor and tumor tissues of the human prostate (Deng et al., 2024). Notably, a higher concentration of polystyrene was observed in tumor tissues compared to the para-tumor tissues (Deng et al., 2024). Exposure to microplastics has been shown to promote the proliferation of skin squamous cell carcinoma in a time- and dose-dependent manner (Wang et al., 2023), disrupt androgen hormone levels, and exacerbate inflammatory response (Barul and Parent, 2021; Kumar et al., 2022). However, the potential impact of polystyrene on the initiation and progression of prostate cancer, as well as the underlying mechanisms, remains to be fully elucidated.

In this study, we explored the possible effects and associated mechanisms of polystyrene (PS) microplastic exposure on the progression of human prostate cancer, utilizing human prostate cancer cell lines and primary cells derived from prostate cancer patients.

2. Materials and methods

2.1. Polystyrene microplastics

Polystyrene microplastics (PS-MPs) with or without green fluorescent (TM-GFC1001 or TM-P1001, diameter: 1 μm, Tomicro) were used for in *vitro* experiments. Keratinocyte Serum Free Medium (K-SFM, 10744019, Gibco, Thermo Fisher Scientific), RPMI 1640 or DMEM medium (Gibco) containing 2 mM L-glutamine, 10% (v/v) fetal bovine serum, and 1% penicillin/streptomycin was used to prepare the PS working solution as described.

2.2. Cell culture and siRNA treatment

Human normal prostate epithelial cells (RWPE-1 cells, CTCC-003-0013, Zhejiang Mason) were maintained in Keratinocyte Serum Free Medium (K-SFM, 10744019, Gibco) and human prostate cancer cell line (LNCaP FGC, CL-0143, Pernosceles) was cultured in 1640 medium at 37C in a humidified incubator with 5% CO_2. Cells with passages 3–8 were used.

For the isolation of primary human prostate tumor cell, excised human prostate tumor were minced into 2 mm^3 pieces and digested for 2 h at 37C in DMEM medium (high glucose) with collagenase II (5 mg/mL) (Invitrogen, Carlsbad, CA), 10 μM Y27632 Rho kinase inhibitor (Abmole Bioscience, Houston, Texas, USA) and 1 nM dihydrotestosterone (Sigma, St. Louis, Missouri, USA). Then, cell suspensions were filtered sequentially through 100 μm and 40 μm cell strainers to remove undigested tissue, and inoculated into cell culture dishes for short-term cultivation.

For Gpx4 siRNA treatment, cells were transfected with Gpx4 siRNA (20 nM) in Lipofectamine™ 3000 Transfection Reagent (Thermo Fisher Scientific) for 48 h. The siRNA was obtained from GenePharma (Shanghai, China), and the sequences are listed in Table S1 (Jin et al., 2023). Knockdown efficiency was evaluated 48 h post-transfection.

2.3. Cell viability assays

To assess cell viability, 5000 cells per well were seeded into 96-well plates and allowed to adhere for 24 h (the absorbance after 48 h of incubation at this density falls within the linear range of 0.2–2.0). Subsequently, polystyrene microplastics (PS) at concentrations ranging from 0.01 to 50 μg/mL were added, and the cells were incubated for an additional 48 h. Cell viability was then determined using the CCK-8 assay (CK04, Dojindo). After adding 10 μL of CCK-8 solution to each well, the plates were incubated for 1.5 h, and the absorbance at 450 nm was measured using a microplate reader (Xu et al., 2020).

2.4. Flow cytometry analysis

To analyze the impact of the indicated treatments on cell survival and apoptosis, cells were stained using either the BeyoClick™ EdU Cell Proliferation Kit (C0071S, Beyotime) or Annexin V-FITC/PI Apoptosis Detection Kit (C1062M, Beyotime), according to the kit operating instructions, followed by flow cytometry analysis. Intracellular reactive oxygen species (ROS) were assessed using the fluorescent probes (5 μM) (DCFH-DA, Beyotime) or C11 BODIPY 581/591 (2 μM) (D3861, Invitrogen) and incubated in the incubator for 30 min (Jin et al., 2023). Following treatment, cells were collected, washed twice with PBS, and analyzed using a CytoFLEX (Beckmann Coulter GmbH, Vienna, Austria). At least 5000 events per sample were recorded. Data were processed using BD FACSDiva Software v7.0 (Becton-Dickinson, USA).

2.5. Cell migration assay

To assess cell motility, cells were seeded into 6-well plates and cultured until reaching approximately 90% confluence. The cells were then scratched with a sterile micropipette tip, and the wells were gently washed with PBS to remove detached cells. Wound closure was monitored under a light microscope (Olympus, Tokyo, Japan) at a 10× magnification. Images were captured at 0 h and after incubation for the designated time. The migratory capacity was quantified by measuring the wound area in three randomly selected fields per sample from each triplicate group (Li et al., 2019). The area of wound closure was calculated as follows: migrated area (%) = (A0 - An)/A0 × 100, A0: the initial wound area, An: the remaining wound area at the point of measurement.

2.6. Transwell

Cells were seeded in 6-well plates and cultured to 80–90 % confluence. Prior to the experiment, the medium was replaced with basal 1640 medium for a 12 h serum starvation treatment. Subsequently, a cell suspension was prepared at a concentration of 10×10^6 cells/mL in basal 1640 medium. Add 100 μL of cell suspension to the upper chamber of the Transwell filter. Fill the lower chamber with complete 1640 medium supplemented with 20 % fetal bovine serum (FBS) as the chemotactic stimulus. Add 0.1 μg/mL PS to the control group. Incubate the plate at 37 °C in a 5 % CO_2 incubator for 12 h. After incubation, carefully remove the upper chamber medium. Gently wipe the upper surface of the membrane with a cotton swab to remove non-migrated cells. Fix migrated cells on the lower surface with 4 % paraformaldehyde for 30 min, then stain with 0.1 % crystal violet for 10 min. Count migrated cells in five randomly selected high-power fields (HPF) under a microscope. Results are expressed as the average count per high-power field.

Invasion: Matrigel was pre-thaw and diluted with basal 1640 (1:8 v/v), 100 μL liquid diluted Matrigel was added into upper chamber and incubated in 37 ℃ for 4 h until it turned to solid gel. The following procedure was the same as migration part.

2.7. RNA extraction and RT-qPCR

Total RNA was isolated from the tissue samples using TRIzol Reagent (Life Technologies). Complementary DNA (cDNA) was synthesized from 1 μg of total RNA using oligo (dT) primers and Moloney Murine Leukemia Virus Reverse Transcriptase (Promega), following the manufacturer's instructions. The primer sequences used for qPCR are listed in Table S1. Quantitative real-time PCR (RT-qPCR) was carried out using the PowerUp™ SYBR™ Green Master Mix (Applied Biosystems, CA, USA) on a QuantStudio 3 Real-Time PCR System (Thermo Scientific, CA, USA). Each 20 μL reaction mixture contained 1 μL of cDNA, 10 μL of SYBR™ Green Master Mix, and 0.2 μM of each primer and were adjusted to the final volume with double distilled H_2O (ddH_2O). β-actin was used as an internal reference gene. The reactions were set up based on the

manufacturer's protocol. PCR conditions were incubation at 50℃ for 2 min and 95℃ for 2 min followed by 40 cycles of thermal cycling (15 s at 95℃ and 1 min at 60℃). Relative expression levels were calculated using the $2^{(-\Delta\Delta Ct)}$ method (Jin et al., 2021).

2.8. Western blotting

Tissue samples or LNCaP cells were lysed in ice-cold RIPA buffer (Beyotime) supplemented with 1 mM phenylmethanesulfonyl fluoride (PMSF). Lysates were centrifuged at 12,000 *g* for 10 min at 4℃, and the supernatants were collected for protein quantification using a BCA Protein Assay Kit (Pierce) (Jin et al., 2021). Equal amounts of protein (40 μg or 25 μg for tissues or LNCaP cell lines, respectively) were denatured, separated on 10 % SDS-PAGE gels, and transferred onto PVDF membrane (Bio-Rad, Hercules, CA, 100 V constant voltage for 90 min).

Membrane were blocked with 5 % non-fat milk in TBST (B1009, Applygen, Applygen Technologies Inc. Beijing, China) for 60 min at room temperature, followed by overnight incubation at 4 ℃ with the following primary antibodies: rabbit polyclonal antibody to PCNA (Proliferating Cell Nuclear Antigen, 1:1000, 10205–2-AP. Proteintech), SOD1/SOD2 rabbit polyclonal antibody (Superoxide Dismutase, 1:1000, Cell Signaling Technology); rabbit polyclonal to TFR (Transferrin, 1:1000, ab82411, Abcam, Cambridge, UK); rabbit polyclonal to FTL (Ferritin light chain, 1:1000, ab69090, Abcam); rabbit monoclonal anti-FTH1 (Ferritin heavy chain, 1:1000, 4393S, Cell Signaling Technology); rabbit monoclonal to GPX4 (Glutathione peroxidase 4, 1:1000, ab125066, Abcam); rabbit monoclonal to ACSL4 (Long-chain fatty acid CoA ligase 4, 1:1000, ab155282, Abcam), rabbit polyclonal to xCT (Cystine/glutamate transporter; Slc7a11, Solute carrier family 7 member 11, 1:1000, ab37185, Abcam), mouse monoclonal to α-tubulin (1:3000, 3873S, Cell Signaling Technology), and mouse monoclonal to β-actin (1:3000, YM3028, ImmunoWay Biotechnology; SuZhou, JiangSu, China), respectively.

After washing, membranes were incubated with HRP-conjugated secondary antibodies (goat anti-rabbit or anti-mouse IgG, 1:5000, Biodragon Immunotechnologies). Protein signals were detected using an ECL kit (Pierce) and visualized with a Tanon 5200 chemiluminescence system. Band intensities were semi-quantified using Image J software (NIH).

2.9. Cell immunofluorescence staining

LnCap cells were seeded in confocal dishes for 24 h and then exposed to 0.1 μg/mL PS with or without green fluorescence for 48 h. After washing with PBST, cell plasma membrane red fluorescence staining kit with PKH26 (C2071M, Beyotime) was added and incubated for 15 min at room temperature away from light. Cells were fixed with 4 % paraformaldehyde for 30 min, permeabilized in PBS containing 1 % Triton X-100 for 20 min at room temperature, and then incubated with blocking buffer (PBS containing 3 % BSA) overnight at 4℃. After incubation, primary antibodies were added and incubated overnight at 4℃: PCNA (Proliferating Cell Nuclear Antigen, 1:1000, 10205–2-AP, Proteintech), PSA (Prostate specific antigen, 1:1000, 5365 T, Cell Signaling Technology). Alexa Fluor-conjugated secondary antibodies were used for detection. Nuclei were stained with DAPI-containing mounting medium. Fluorescence was visualized using a Zeiss LSM 710 confocal microscope.

2.10. Iron staining

2×10^5 LnCap cells were cultured in glass bottom dishes (BS-20-GJM, Life sciences) and treated with PS. Following treatment, cells were washed 3 times in HBSS, and incubated with 1 μM FerroOrange (F374, dojindo) in HBSS for 30 min at 37℃ in a 5 % CO_2 atmosphere. Fluorescence was detected using a Zeiss LSM 710 confocal microscope with a 20 × objective. Images (512 × 512 pixels) were captured under identical exposure conditions using the Cy3 filter set (ex: 514 nm, em: 525–596 nm) (Weber et al., 2020).

2.11. Hematoxylin and eosin (H&E) staining

Fresh prostate cancer tissues were fixed in testicular tissue fixative (G1121, Servicebio, Wuhan, China) for 24 h, dehydrated through an ethanol gradient, the fixed testes were embedded in paraffin and then sectioned (5μm-thick) were cut, deparaffinized, and stained with H&E as previously described (Luo et al., 2023). Histological changes were analyzed using a digital panoramic scanner (WS-10, WISLEAP, Zhiyue Medical Technology Co., LTD; Jiangsu, China).

2.12. Immunofluorescence staining of sections

The paraffin sections were heated at 95℃ in EDTA antigen repair buffer (ZLI-9071, ZSGB-BIO; Beijing, China) for 30 min and cooled to room temperature. Sections were blocked with 10 % donkey serum (0.3 % Triton X-100 in PBS) for 1 h at room temperature, followed by overnight incubation at 4℃ with primary antibodies as described. Secondary antibodies were applied for 1 h at room temperature, and nuclei were counterstained with DAPI (100 ng/mL, Beyotime, Jiangsu, China). Sections were mounted with Gel-Mount and imaged using a confocal microscope (Zeiss LSM710, Carl Zeiss Microscopy GmbH, Jena, Germany) (Jin et al., 2023).

2.13. Oxidative stress assessments

Intracellular oxidative stress levels were assessed using commercial kits from Beyotime Biotechnology according to the manufacturer's instructions as described before (Luo et al., 2023), including assays for total antioxidant capacity (cat# S0119), glutathione peroxidase (GPx) (cat# S0058, total glutathione peroxidase assay kit with NADPH), superoxide dismutase (SOD) (cat# S0109, total superoxide dismutase assay kit with NBT), GSH and GSSG (reduced glutathione, GSH; oxidized glutathione disulfide, GSSG; cat# S0053, GSH and GSSG assay kits), and malondialdehyde (MDA) (cat# S0131M, lipid peroxidation MDA assay kit).

2.14. Transcriptome profiling

Total RNA was extracted from LNCaP cells and tissue samples using TRIzol (Invitrogen). The cDNA samples were sequenced using the Agilent Bioanalyzer 2100 system (Agilent Technologies, CA, USA). The clustering of the index-coded samples was performed on a cBot cluster generation system using HiSeq PE Cluster Kit v4-cBot-HS (Illumina) according to the manufacturer's instructions. After cluster generation, the libraries were sequenced on an Illumina platform and 150 bp paired-end reads were generated. Sequencing was performed using the NovaSeq 6000 S4 Reagent kit V1.5 (Jin et al., 2023).

2.15. Multiplex cytokine assay

Luminex multiplex beads assay (Luminex 200 system, Luminex Corporation, Austin, TX, USA) was used to quantify cytokine levels in cell supernatants. Briefly, supernatants were incubated with capture bead mix for 2 h at room temperature, followed by detection antibody and streptavidin-PE incubation for 30 min. Data were acquired using the Luminex 200™ analyzer (Luminex, Austin, TX, USA), and normalized to total protein content (PC0020, Solarbio, Beijing, China) (Yi et al., 2023).

2.16. Statistical analysis

All statistical analyses were conducted using GraphPad Prism 9.0 (GraphPad Software, La Jolla, CA). All quantitative biochemical data and immunofluorescence staining were representative of at least three independent experiments. Two-tailed unpaired Student's *t* test or

Wilcoxon test was used for the comparison of the mean values between two groups. One-way ANOVA with Sidak's *post hoc* test was used for multiple comparisons. All data were expressed as means ± SEM, and differences with $P < 0.05$ were considered statistically significant. The significant differences between groups were represented as $^{*}P < 0.05$, $^{**}P < 0.01$, and $^{***}P < 0.001$.

3. Results

3.1. Low-dose of PS microplastic exposure promotes the cell proliferation and migration of prostate cancer cells

We first assessed the impact of PS on the viability of normal prostate epithelial cells (RWPE-1). Our results revealed that PS exposure could inhibit the proliferation of RWPE-1 cells in both a time- and dose-dependent manner (Fig. 1A). Intriguingly, a similar trend was observed in prostate cancer cells (LNCaP FGC cells, LNCaP), where PS exposure exhibited a comparable time- and dose-dependent effect on cell viability. Immunofluorescence imaging confirmed that PS particles could cross the cell membrane and enter the LNCaP cells (Fig. 1B). Exposure to a moderate concentration of PS (0.1 μg/mL) for 48 h (referred to as PS exposure) significantly enhanced the proliferation of LNCaP, whereas other concentrations or exposure durations generally suppressed cell proliferation (Fig. 1C). These findings suggest that low concentrations of PS exposure may be able to promote the proliferation of LNCaP cells.

To further investigate this proliferative effect, we examined the expression of key cell proliferation markers. Immunofluorescence staining and Western blot results demonstrated increased protein expression of proliferating cell nuclear antigen (PCNA) in PS-exposed LNCaP cells (Fig. 1D-E and Figure S1). These results were further supported by a significant increase in the average fluorescence intensity of EdU-488 in these cells, indicating enhanced DNA synthesis (Fig. 1G). Co-exposure of PS and di-(2-ethylhexyl)phthalate induced DNA damage and cell cycle arrest in mouse ovarian granulosa cells through promoting the ROS production (Wu et al., 2023) Therefore, we also evaluated the effects of PS exposure on LNCaP cell cycle and apoptosis. No significant differences were identified in cell cycle and apoptosis between groups (Figure S1), but PS exposure did promote the migration and invasion of LNCaP over time through scratch and transwell assays (Fig. 1I-K). Collectively, these data suggested that low-dose of PS exposure may promote LNCaP cell proliferation through mechanisms independent of apoptosis or cell cycle regulation.

3.2. Low-dose of PS microplastic exposure upregulates oxidative stress levels of prostate cancer cells

Previous study has shown that mild oxidative stress could promote cell proliferation (Cheng et al., 2024). To explore whether PS influence oxidative stress levels in LNCaP cells, we first employed Luminex liquid-phase suspension microarrays to assess the expression of inflammatory cytokines. Our results revealed that the expression of Eotaxin, IL-4, IL-12 and IFN-γ was significantly changed in the PS group (Fig. 2A). These chemokines are primarily involved in eosinophil recruitment and immune modulation, with IL-4 inhibiting Th1 cell-mediated inflammatory response while IL-12 and IFN-γ promote Th1 cell differentiation and enhance cellular immune response. These results suggest that PS exposure can alter the levels of some cytokines in LNCaP cells.

We further investigated the impact of PS on oxidative stress. Our data revealed that the malondialdehyde (MDA) level of PS group was significantly elevated (Fig. 2B). PS exposure also up-regulated the GSH/GSSG level, protein expression of SOD1/2, and total antioxidant capacity of LNCaP cells although the superoxide dismutase activity and glutathione peroxidase activity remained unchanged (Fig. 2C-I and Figure S2). Consistently, the levels of oxidative stress production such as ROS and lipid peroxidation were also increased (Fig. 2J-K) in PS-exposed LNCaP cells.

3.3. Combined analysis of RNA sequencing data from PS microplastic-treated LNCaP cells and human prostate cancer tissues

To uncover the molecular mechanisms underlying the promotion of PS on prostate cancer cell proliferation, we performed a combined analysis of RNA sequencing data from PS-treated LNCaP cells and human prostate cancer tissues. Detailed patient clinical characteristics are summarized in Table S3. Principal component analysis (PCA) results revealed distinct gene expression profiles between vehicle and PS-treated LNCaP cells, as well as between human prostate para-tumor and tumor tissues (Fig. 3A-B). Among them, there were 144/13, 142/133 significantly down or up-regulated genes in the PS group or human prostate tumor tissues, respectively (Fig. 3C-D). We further analyzed these differentially expressed genes to find the enriched up- and down-regulated pathways, and the Venn diagram demonstrated 5/62 down- or up-regulated pathways (Fig. 3E-F). The overlapped down-regulated pathways, including cytokine-cytokine receptor interaction, apoptosis, and NF-kappa B signaling pathway, are known to regulate inflammation, immune response, and programmed cell death. In contrast, the up-regulated pathways such as glutathione metabolism, arginine biosynthesis, and glycine, serine and threonine metabolism, which are involved in protein synthesis, nitric oxide production, cellular antioxidant defense, and redox homeostasis, are closely related to cell survival and stress response (Fig. 3G-H). The heat map further visualized a subset of differentially expressed genes in these pathways (Fig. 3I-J). As aforementioned, the ratio of GSH/GSSG and the abundance of MDA were increased in PS-treated cells (Fig. 2B and D), while the apoptosis was unaffected. Combined with the overlapped KEGG pathways, these findings suggest that glutathione metabolism-regulated ferroptosis may play a crucial role in mediating proliferative effects of low-dose of PS exposure in both LNCaP cells and human prostate tumor cells.

3.4. Low-dose of PS microplastic exposure inhibited ferroptosis of prostate cancer cells

To investigate whether the proliferative effect of PS is associated with altered ferroptosis, we analyzed the expression of ferroptosis-related proteins in human prostate tumor tissues. Western blot result showed that the expression levels of glutathione peroxidase 4 (GPX4) and acyl-CoA synthetase long-chain family member 4 (ACSL4) were significantly up-regulated or down-regulated in the tumor tissues compared with their paired para-tumor tissues, while the expression of cystine/glutamate transporter protein (SLC7A11), transferrin (TFR1), ferritin heavy chain (FTH1) and ferritin light chain (FTL) was not significantly altered (Fig. 4A and Figure S3). Combined HE staining and immunofluorescence staining also showed an increase or decrease in expression of GPX4 and ACSL4 in the tumor region (Fig. 4C). We further examined the changes in iron ion abundance in human prostate tumor tissues. Fe^{2+} and total iron ions were significantly higher in tumor tissues compared with para-tumor tissues. However, there was no significant difference in the ratio of Fe^{2+}/Fe^{3+} (Fig. 4D-G).

In LNCaP cells, Western blot analysis showed that the protein expression levels of GPX4, SLC7A11, ACSL4 and FTH1 were significantly up-regulated in the PS group compared with the vehicle controls, while the protein expression of TFR1 and FTL remained unchanged (Fig. 4H and Figure S4). The Fenton reaction, triggered by intracellular iron ion accumulation exceeding cellular self-regulatory capacity, induces cellular ferroptosis. Thus, we used an iron staining kit to detect Fe^{2+} content in LNCaP FGC cells and found that Fe^{2+} accumulation in LNCaP cells was significantly reduced in the PS group compared with the vehicle group (Fig. 4I), indicating that low-dose of PS exposure suppresses ferroptosis in prostate cancer cells.

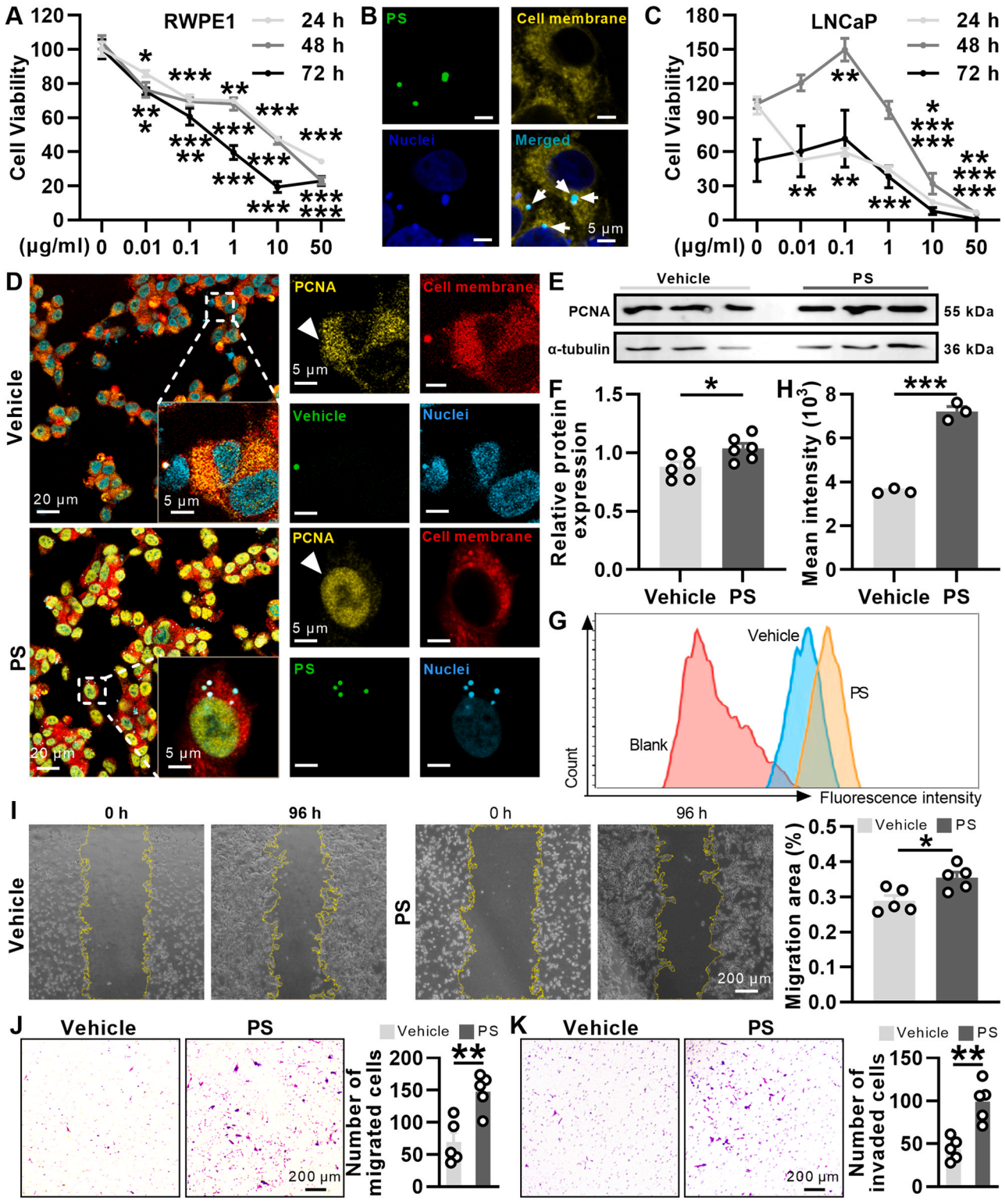

Fig. 1. Effect of low-dose PS microplastic exposure on the proliferation and migration of prostate cancer cells. A-C. Changes in cell viability of two cell lines (RWPE-1 and LNCaP) after exposure to different concentrations of PS (polystyrene) for different periods of time (24 h, 48 h, and 72 h), biological replicates, n = 7/group. B. Co-localization of PS, cell membranes, and nuclei, with arrows pointing to the polystyrene. Yellow: PCNA, green: PS, red: cell membrane, blue: nucleus. Scale bar 5 μm. D. Immunofluorescence staining of cellular PCNA, arrowheads point to PCNA. yellow: PCNA, green: PS, red: cell membrane, blue: nucleus. Scale bar 20 μm. bottom left and right panels are enlargements of the dashed box in the left panel with a scale bar of 5 μm. E-F. Western blot representative maps and quantitative analysis of PCNA protein expression in LNCaP FGC cells with different treatments. biological replicates, n = 3/group. G-H. Representative graphs and statistical graphs of fluorescence intensity of LNCaP cells with different treatments detected by EdU-488. biological replicates, n = 3/group. I. Representative graphs of cell migration and statistical graphs of cell migration area for the two groups at different time points (0 h and 96 h). biological replicates, n = 3/group. PCNA, proliferating cell nuclear antigen. J. Changes in number of migrated cells after exposure to PS (polystyrene) for 72 h, biological replicates, n = 5/group. K. Changes in number of invaded cells after exposure to PS (polystyrene) for 72 h, biological replicates, n = 5/group. All data are presented as mean ± SEM. *, $P < 0.05$; **, $P < 0.01$; ***, $P < 0.001$. Unpaired t test for (F) and (H-I); one-way ANOVA with Sidak's *post-hoc* test for (A) and (C).

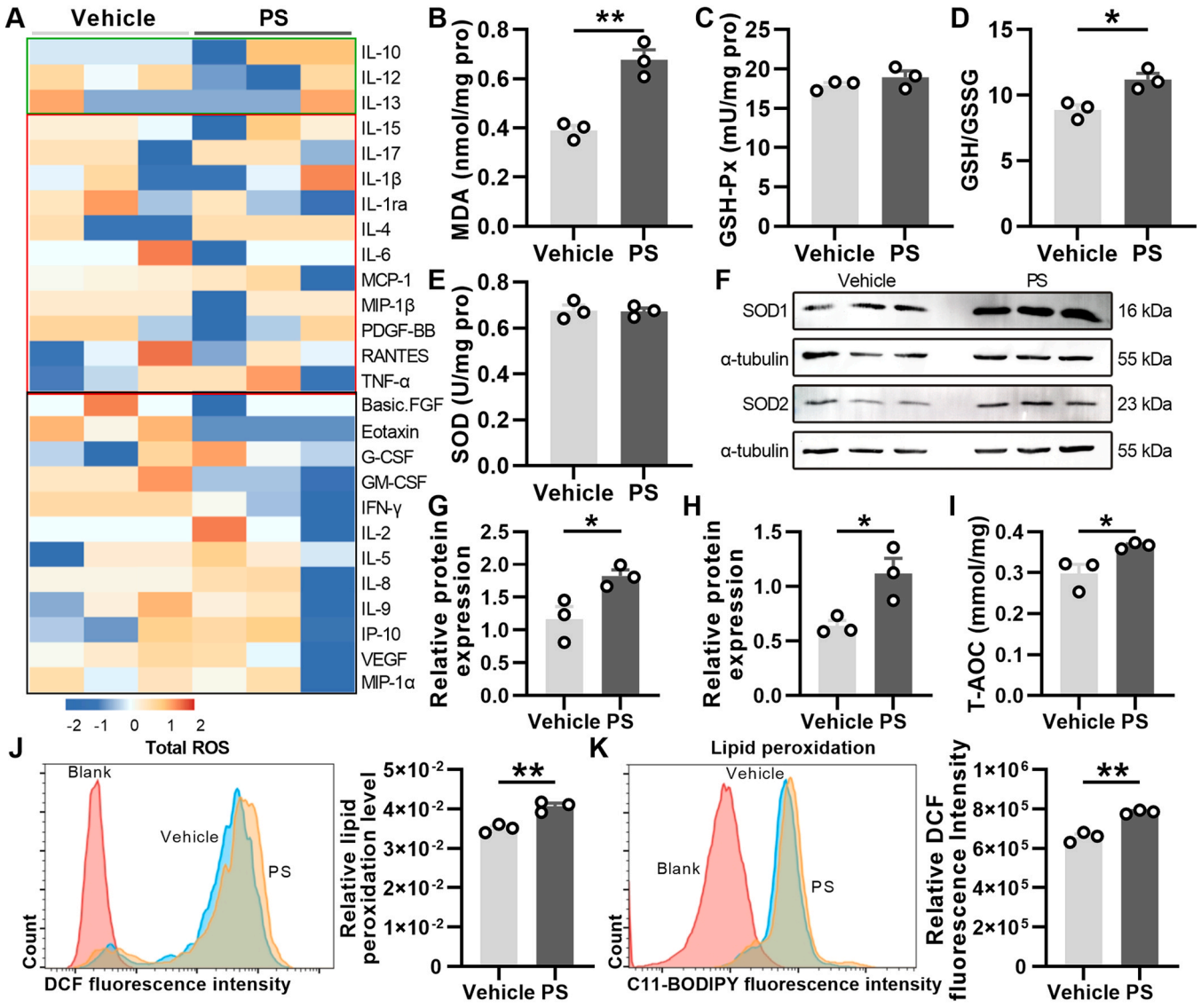

Fig. 2. Low-dose PS microplastic exposure upregulated oxidative stress levels in prostate cancer cells. A. Heatmap of cytokine expression levels, with anti-inflammatory factors in blue, pro-inflammatory factors in red, and other factors in black. B-E. Changes in malondialdehyde (MDA), glutathione peroxidase activity (GSH-Px), glutathione/oxidized glutathione ratio (GSH/GSSG), and superoxide dismutase activity (SOD) levels; biological replicates, n = 3/group. F-H. SOD1/2 protein expression analysis of control (Vehicle) and PS-treated (PS) cells, biological replicates, n = 3/group. I. Changes in total antioxidant capacity (T-AOC) levels, biological replicates, n = 3/group. J. ROS levels of LNCaP FGC cells in different treatments and unstained negative control, biological replicates, n = 3/group. K. Lipid peroxidation levels of LNCaP FGC cells in different treatments and unstained negative control, biological replicates, n = 3/group. VEH, Vehicle; IL, interleukin. MCP, monocyte chemoattractant protein; MIP, macrophage inflammatory protein; PDGF, platelet-derived growth factor; RANTES, regulated upon activation normal T cell expressed and secreted; TNF, tumor necrosis factor; basic FGF, basic fibroblast growth factor; G-GSF, granulocyte colony-stimulating factor; GM-GSF, granulocyte macrophage colony-stimulating factor; IFN, interferon; VEGF, vascular endothelial growth factor. All data are presented as mean ± SEM. *, $P < 0.05$; **, $P < 0.01$. Unpaired *t* test for (B-E), and (G-K).

3.5. Knockdown of GPX4 prevents PS microplastic exposure-mediated ferroptosis in LNCaP cells

Given the observed downregulation of GPX4 in both human prostate cancer tissues and PS-exposed LNCaP cells, we sought to determine whether PS exposure promotes LNCaP cell proliferation via GPX4-mediated ferroptosis. To this end, GPX4 was knockdown in LNCaP cells, followed by PS exposure. Firstly, transfection efficiency was confirmed by Western blot, showing the siRNA (si-NC: Negative control, and si-GPX4: siRNA-GPX4) had high transfection efficiency (Fig. 5A), GPX4 protein expression was also significantly decreased compared with Si-NC group (Fig. 5B-C and Figure S5). Next, we found that GPX4 protein expression was significantly down-regulated in the si-GPX4 +PS group compared with the si-NC+PS group (Fig. 5D and Figure S6). We then examined the alteration of intracellular ROS levels and lipid peroxidation levels, and found significantly elevated cellular ROS levels and lipid peroxidation levels in si-GPX4 +PS group compared with the control group (Fig. 5G-H). Consistently, Fe^{2+} accumulation was increased in the si-GPX4 +PS group compared with the si-NC+PS group (Fig. 5I). These findings suggest that PS exposure could promote the proliferation of LNCaP cells through inhibiting GPX4-mediated ferroptosis.

3.6. Low-dose PS microplastic exposure inhibit ferroptosis in human prostate cancer progenitor cells

To further validate the detailed molecular mechanism underlying PS-induced cells proliferation, we isolated and extracted the prostate cancer

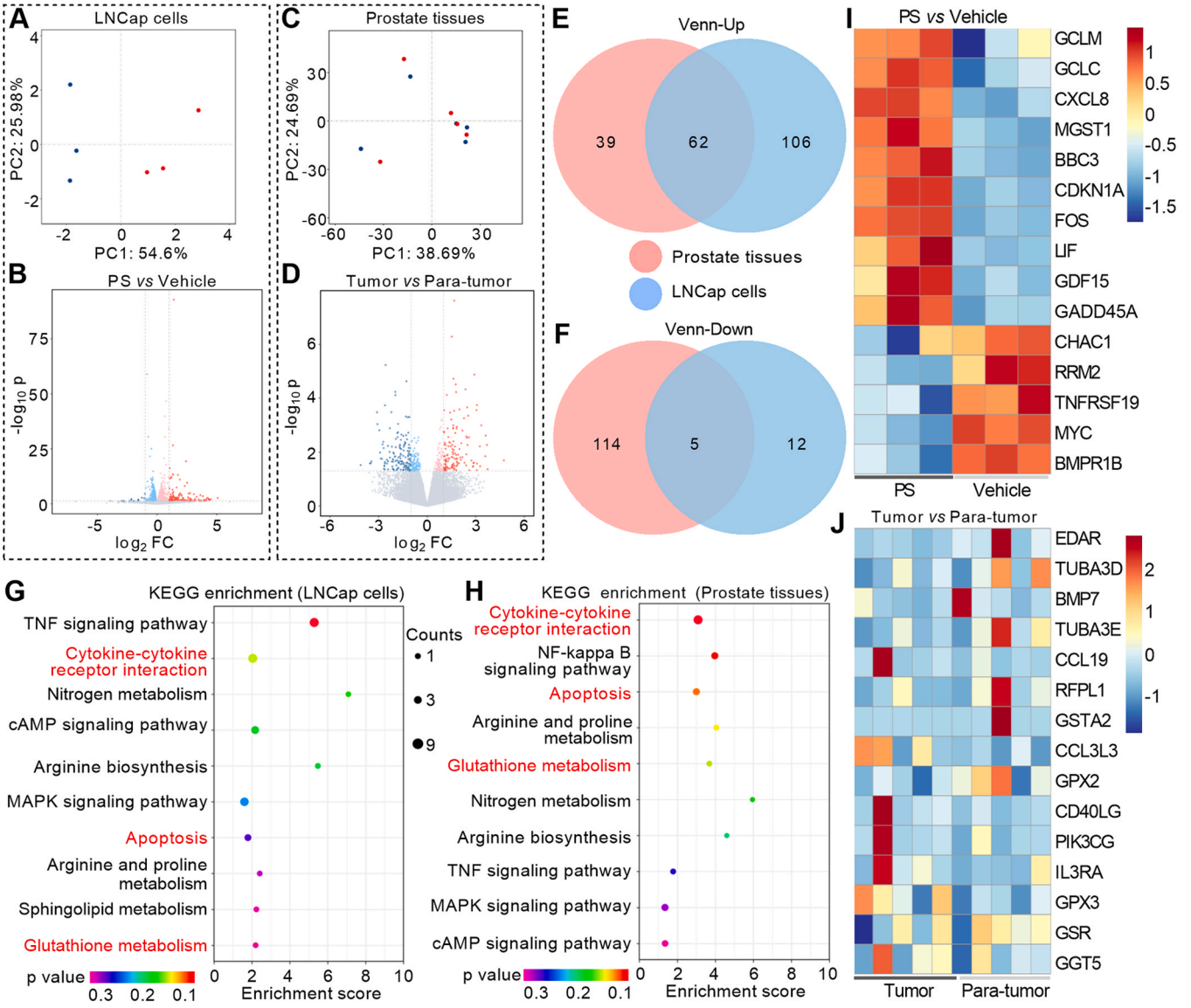

Fig. 3. Combined analysis of RNA sequencing data from PS microplastic-treated LNCaP cells and human prostate cancer tissues. A-B. PCA results comparing vehicle with PS-treated LNCaP cells, biological replicates, n = 3/group, and comparing human prostate para-tumor with tumor tissues, biological replicates, n = 5/group. C-D. Differential gene volcano maps comparing vehicle with PS-treated LNCaP cells, and comparing human prostate para-tumor with tumor tissues. E-F. Venn diagrams of down-regulated and up-regulated differential gene enrichment pathways. G-H. Top 10 enrichment pathways in LNCaP cells and human prostate tissues. Red font indicates pathways associated with cell survival and stress response. I-J. Heat map of pooled differentially expressed genes from LNCaP cells and human prostate tissue-associated pathways. GCLM, glutamate-cysteine ligase modifier; GCLC, glutamate-cysteine ligase catalytic; CLCX8, chemokine ligand 8; MGST1, microsomal glutathione S-transferase 1; BBC3, BCL2 binding component 3; CDKN1A, cyclin dependent kinase inhibitor 1A; FOS, fos proto-oncogene; LIF, leukemia inhibitory factor; GDF15, growth differentiation factor 15; GDAA, growth arrest and DNA damage; CHAC1, cysteine hydrolase anti-oxidant pathway protein 1; RRM2, ribonucleotide reductase M2; TNFRSF19, tumor necrosis factor receptor superfamily 19; MYC, myelocytomatosis oncogene; BMPR1B, bone morphogenetic protein receptor type 1B; EDAR, ectodysplasin A receptor; TUBA, tubulin alpha; BMP, bone morphogenetic protein; CCL, C-C motif chemokine ligand; RFPL1, ret finger protein like 1; GSTA2, glutathione S-transferase alpha 2; GPX, glutathione peroxidase; CD40LG, CD40LG, cluster of differentiation 40 ligand; PIK3CG, phosphatidylinositol-4,5-bisphosphate 3-kinase catalytic subunit gamma; GSR, glutathione-disulfide reductase; GGT5, gamma-glutamyltransferase 5.

progenitor cells through tissue digestion and we found nearly all cells were prostate-specific antigen (PSA) positive cells (Fig. 6A). Detailed clinical characteristics of patients are summarized in Table S3. Subsequently, we examined the lipid peroxidation level of the primary cells and found that PS exposure led to an increase in the lipid peroxidation level of the primary cells (Fig. 6B), accompanied by upregulated expression of ACSL4 and GPX4 (Fig. 6C and Figure S6). Consistently, Fe^{2+} accumulation was also increased in primary cells after exposure to PS (Fig. 6D-E).

4. Discussion

Numerous studies have demonstrated that microplastics, as an emerging class of environmental pollutants, are capable of entering the human body through multiple exposure routes such as inhalation, ingestion and dermal contact due to their small size and distinct physicochemical properties (Zhang et al., 2020). Once internalized, these particles can bypass physiological defense mechanisms and accumulate in various organs (Zhu et al., 2024). For instance, in the gastrointestinal tract, microplastics may enter systemic circulation after intestinal absorption and subsequently accumulate in organs such as the liver and

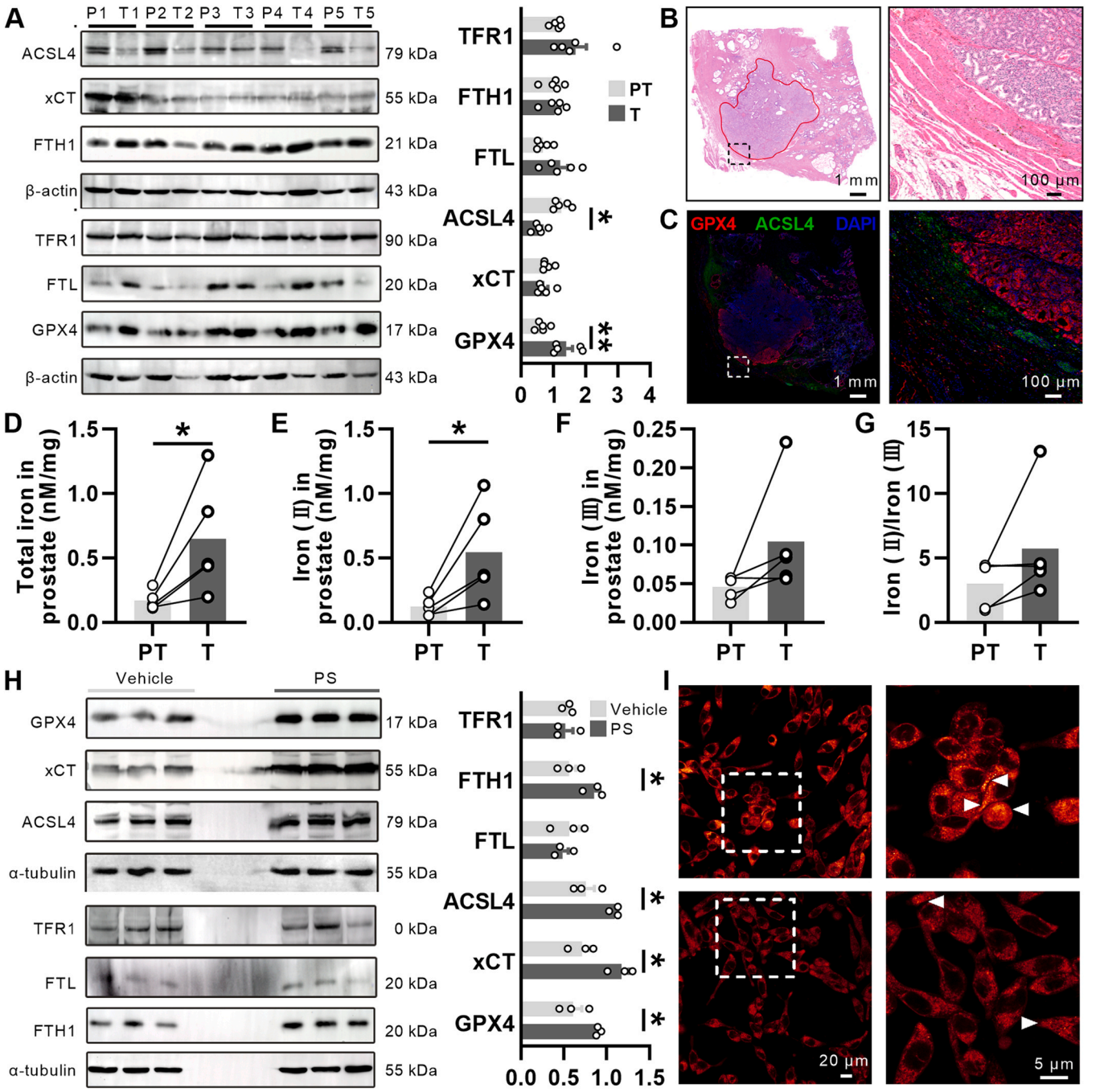

Fig. 4. Low-dose PS microplastic exposure inhibited ferroptosis of prostate cancer cells. A. The expression of ferroptosis-related protein in human prostate tumor tissues, biological replicates, n = 5/group. B-C. Representative graphs of HE staining and immunofluorescence staining of GPX4/ACSL4 in prostate cancer paracellular and cancerous tissues. Scale bars are 1 mm and 100 μm, respectively. red line area represents cancer tissues, red area represents GPX4, and green area represents ACSL4. D-G. The changes of iron ion abundance in human prostate tumor tissues, biological replicates, n = 4/group. H. The changes in expression of ferroptosis-related proteins in LNCaP cells, biological replicates, n = 3/group. I. Representative graphs of iron ion staining in LNCaP cells with different treatments, scale bars are 5 μm and 20 μm, respectively. Above: Vehicle, below: PS, The white arrows in the graph represent cells with Fe^{2+} accumulation. PT, para-tumor; T, tumor. All data are presented as mean ± SEM. *, P < 0.05; **, P < 0.01. Paired samples *t* test for (D-G); one-way ANOVA with Sidak's *post-hoc* test for (A) and (H).

spleen (Chen et al., 2022). In the respiratory system, inhaled microplastic particles can deposit in lung tissues, and chronic exposure may contribute to pulmonary pathologies (Lu et al., 2023). Even in the reproductive system, the presence of microplastics has been reported, raising concerns about potential impact on reproductive health (He and Yin, 2024).

In the present study, we observed that low-dose PS (polystyrene) exposure promoted the proliferation of LNCaP cells. Many studies have shown that microplastics at high concentrations or under specific conditions have toxic effects which they inhibit cell growth and induce apoptosis (Yong et al., 2020). For example, PS is cytotoxic only at high concentrations and induces metabolic changes and endoplasmic reticulum stress in human bronchial epithelial cell lines (Lim et al., 2019). The low-dose PS exposure in this study promoted the proliferation of LNCaP cells, upregulated PCNA protein expression, and increased DNA synthesis. Previous studies have shown that microplastics can elevate mitochondrial ROS levels, alter mitochondrial membrane potential, trigger the release of mitochondrial DNA into the cytoplasm, and

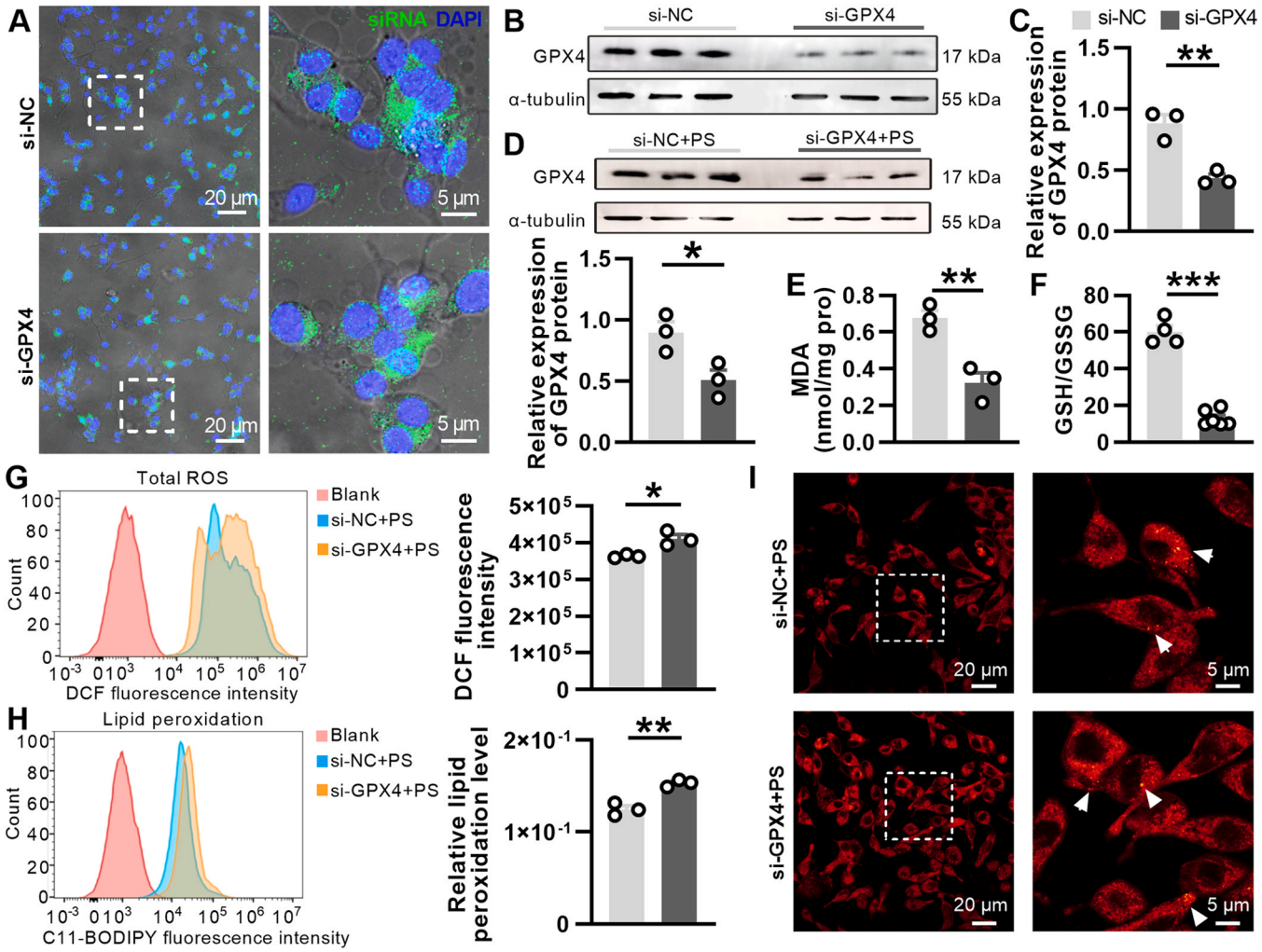

Fig. 5. Knockdown of GPX4 prevents PS microplastic exposure-mediated ferroptosis in LNCaP cells. A. Representative plots of transfection efficiency of negative control and siRNA-GPX4 with scales of 20 μm and 5 μm. green: siRNA, blue: nucleus. B-C. Representative graph (B) and statistical graph (C) of GPX4 protein expression, biological replicates, n = 3/group. D. The GPX4 protein expression level in the si-NC+PS group and the si-NC+PS group, biological replicates, n = 3/group. E-F. Statistical graphs of MDA and GSH/GSSG levels in cells of both groups, biological replicates, n = 3–6/group. G. Representative graphs and statistical graphs of ROS levels, biological replicates, n = 3/group. H. Representative graphs and statistical graphs of lipid peroxidation levels, biological replicates, n = 3/group. I. Representative graphs of iron ion staining in cells of both groups, with scales of 5 μm and 20 μm, respectively. The white arrows in the graph represent cells with Fe^{2+} accumulation. All data are presented as mean ± SEM. *, P < 0.05; **, P < 0.01; ****, P < 0.0001. Unpaired *t* test for (C-H).

activate NLRP3 inflammasome, ultimately promoting skin cancer cell proliferation (Wang et al., 2023). We hypothesized that low-dose PS exposure induces cellular stress response that activates certain intracellular proliferation-related signaling pathways promoting the proliferation of LNCaP cells.

Our results further indicated that PS exposure increased oxidative stress and ROS levels while upregulating protein expression of SOD1/2 in LNCaP cells. A complex regulatory relationship exists between oxidative stress and cell proliferation, whereas moderate levels of oxidative stress may promote cell proliferation by activating relevant signaling pathways (Zeng et al., 2023). It is possible that PS exposure may protect against oxidative damage by modulating cellular redox homeostasis, activating antioxidant stress response elements such as Nrf2, and up-regulating SOD1/2 expression (Di Chiano et al., 2024). When oxidative stress exceeds a certain threshold, it causes damage to cells. In this study, PS induced a mild oxidative stress response in cells, which likely promoted cell proliferation.

In addition, we observed significant alterations in the expression of several inflammatory cytokines following PS exposure in LNCaP cells: eotaxin, IFN-γ, and IL-12 expression was down-regulated, while IL-4 was up-regulated. Inflammatory mediators play a key role in tumor microenvironment and can influence cancer cell proliferation, migration, and immune evasion (Chavez-Dominguez et al., 2021). The observed increase in IL-4 expression may activate the JAK-STAT6 signaling pathway and promote the proliferation and cancer cell survival (Sarapultsev et al., 2023). Conversely, the reduced levels of eotaxin, IFN-γ, and IL-12 may impair immune surveillance, potentially allowing cancer cells to escape immune recognition and facilitating tumor progression (Xue et al., 2023).

Pathway analysis revealed the involvement of several key signaling cascades in the cellular response to PS exposure. The phosphoinositide 3-kinase (PI3K)/protein kinase B (AKT) pathway emerged as a central mediator of microplastic-induced effects. Upon activation, PI3K phosphorylates AKT, which in turn inhibits pro-apoptotic proteins Bad (BCL2 Associated Agonist of Cell Death) and enhances the expression of anti-apoptotic factors Bcl-2 (B-cell lymphoma-2), thereby suppressing apoptosis and promoting cell survival and proliferation (Shorning et al., 2020). Moreover, AKT can activate the mTOR (mammalian target of rapamycin) pathway to regulate cellular metabolism and growth (Edlind and Hsieh, 2014). In parallel, mitogen-activated protein kinases (MAPK)/extracellular signal-regulated kinases (ERKs) pathway may also be activated by microplastics; phosphorylated ERK1/2 translocate to the

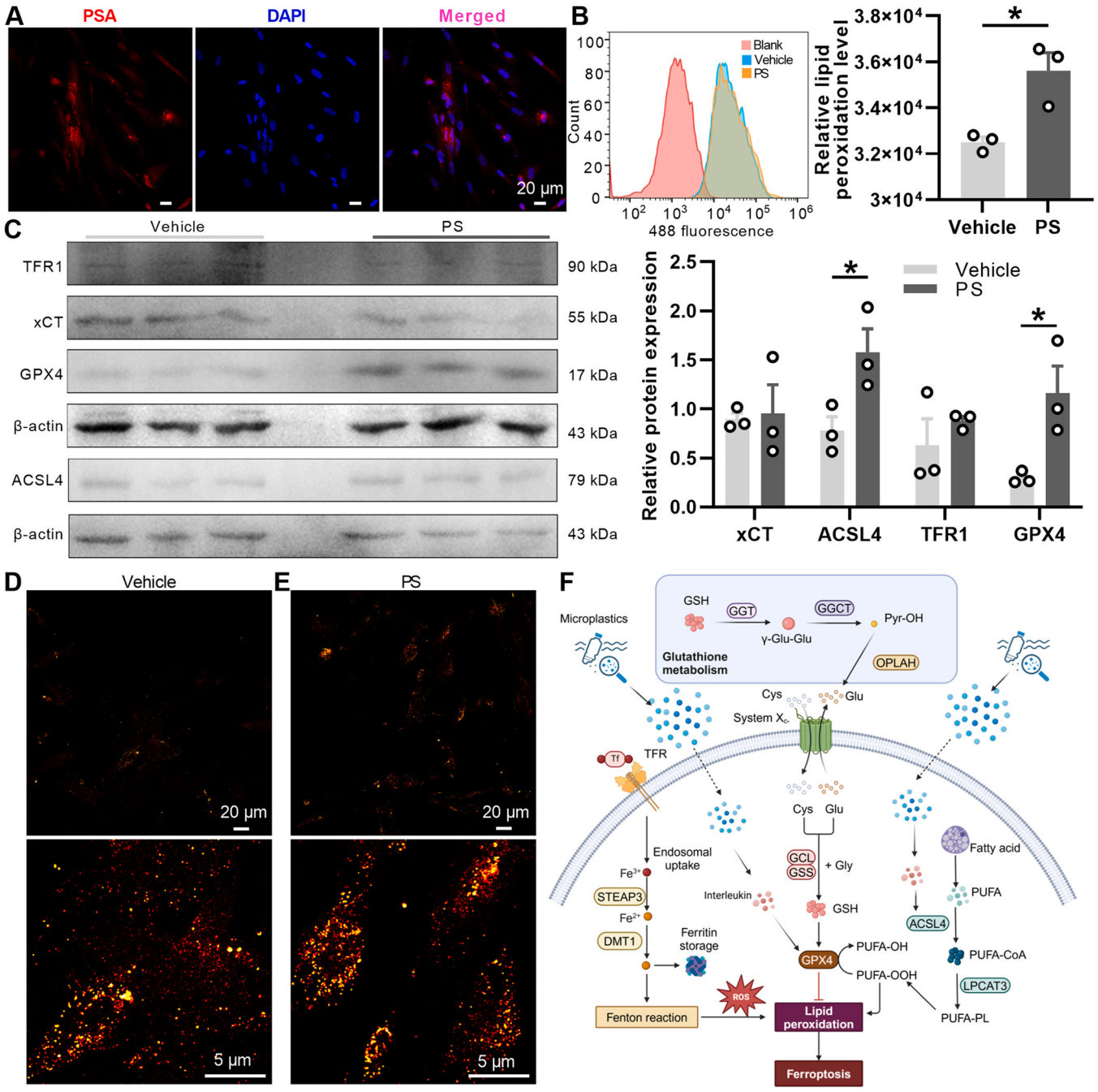

Fig. 6. Low-dose PS microplastic exposure inhibits ferroptosis in human prostate cancer progenitor cells. A. Immunofluorescence staining identification of human prostate cancer progenitor cells specific antigen, scale bar is 20 μm. red: PSA, blue: nucleus. B. The lipid peroxidation level in primary cells, biological replicates, n = 3/group. C. The expression of ferroptosis-related protein in primary cells, biological replicates, n = 3/group. D-E. Representative graphs of iron ion staining in primary cells with scales of 5 μm and 20 μm, respectively. F. Graphical abstract. PS microplastic influences prostate cancer cell development via ferroptosis. By promoting the expression of GPX4, it enhances the antioxidant capacity and inhibits the ferroptosis of cells, thus promoting cell proliferation. PSA, prostate specific antigen; STEAP3, six-transmembrane epithelial antigen of the prostate 3; DMT1, divalent metal transporter 1; GCL, glutamate cysteine ligase; GSS, glutathione synthetase; PUFA, polyunsaturated fatty acid; LPCAT3, Lysphosphatidylcholine acyltransferase 3; ACSL4, acyl-CoA synthetase long chain family member 4; GPX4, glutathione peroxidase 4; ROS, reactive oxygen species. All data are presented as mean ± SEM. *, $P < 0.05$. Unpaired *t* test for (B); one-way ANOVA with Sidak's *post-hoc* test for (C).

nucleus, modulates transcription factor activity, and promotes the expression of genes related to cell proliferation (Xiong et al., 2025).

Our study further suggests that PS influences prostate cancer cell development via ferroptosis. By promoting the expression of GPX4, it enhances cellular antioxidant defenses and suppressing ferroptosis of cells, thus promoting cell proliferation. There may be complex interactions and cross-regulation between these pathways, which together influence the cellular response to PS stimulation. Notably, integrated analysis of clinical samples and in vitro experiments revealed the presence of microplastics in both human prostate para-tumor and tumor tissues, with significant differences in polymer composition and abundance. These observations support the hypothesis that PS microplastics may promote prostate cancer progression through the modulation of ferroptosis (Fig. 6F). This study has several limitations. The direct

addition of microplastics to the culture medium does not accurately represent the exposure route in human beings. Additionally, short-term low-dose exposure cannot accurately represent everyday exposure. In this study, we conducted only in vitro experiments. Future research should explore in vivo experiments to make the results more convincing. Therefore, further studies are needed to bridge the gap between experimental and environmental conditions to comprehensively evaluate the human health implications of polystyrene microplastics exposure.

5. Conclusions

In this study, we present multiple pieces of evidence demonstrating that low-dose PS (polystyrene) microplastics promotes the proliferation of prostate cancer cells and modulates inflammatory responses and oxidative stress levels in prostate cells. Through integrated transcriptomic analyses of both cell models and human prostate tissues, we identified potential molecular mechanisms underlying these effects. The findings were further validated using gene expression assays and primary cell culture experiments. Our results indicate that low-dose polystyrene exposure promotes human prostate cancer cell proliferation through GPX4-mediated ferroptosis. These findings suggest that polystyrene microplastics can promote the development of prostate cancer, providing a new perspective for research into the etiology of prostate cancer.

CRediT authorship contribution statement

Zirun Jin: Writing – original draft, Supervision, Project administration, Funding acquisition. **Jia Zheng:** Supervision, Funding acquisition. **Hui Jiang:** Funding acquisition, Conceptualization. **Zidi Yan:** Formal analysis, Data curation. **Chenyao Deng:** Writing – original draft, Visualization, Data curation. **Jingmo Li:** Writing – original draft, Visualization, Methodology, Data curation. **Wenyu Zou:** Investigation, Formal analysis, Data curation, Writing – review & editing. **Yinuo Dong:** Formal analysis, Data curation. **Xindi Jiang:** Writing – review & editing, Validation.

Data sharing statement

Data are available on request from the authors.

Declaration of Competing Interest

The authors declare that they have no known competing financial interests or personal relationships that could have appeared to influence the work reported in this paper.

Acknowledgements

This work was supported by National Key Research & Development Program of China (2024YFC2706800, 2022YFC2702600). Non-communicable Chronic Diseases-National Science and Technology Major Project (2024ZD0530200), Beijing Municipal Natural Science Foundation (L256060 and L248047), and the National Natural Science Foundation of China (Grant No. 82495191 and No. 82271630).

Appendix A. Supporting information

Supplementary data associated with this article can be found in the online version at doi:10.1016/j.ecoenv.2025.119285.

Data availability

Data will be made available on request.

References

Almeeri, M.N.E., Awies, M., Constantinou, C., 2024. Prostate cancer, pathophysiology and recent developments in management: a narrative review. Curr. Oncol. Rep. 26 (11), 1511–1519.
Barul, C., Parent, M.E., 2021. Occupational exposure to polycyclic aromatic hydrocarbons and risk of prostate cancer. Environ. health a global access sci. sour. 20 (1), 71.
Bergengren, O., Pekala, K.R., Matsoukas, K., Fainberg, J., Mungovan, S.F., Bratt, O., Bray, F., Brawley, O., Luckenbaugh, A.N., Mucci, L., Morgan, T.M., Carlsson, S.V., 2023. 2022 update on prostate cancer epidemiology and risk Factors-A systematic review. Eur. Urol. 84 (2), 191–206.
Center, M.M., Jemal, A., Lortet-Tieulent, J., Ward, E., Ferlay, J., Brawley, O., Bray, F., 2012. International variation in prostate cancer incidence and mortality rates. Eur. Urol. 61 (6), 1079–1092.
Chartres, N., Cooper, C.B., Bland, G., Pelch, K.E., Gandhi, S.A., BakenRa, A., Woodruff, T. J., 2024. Effects of microplastic exposure on human digestive, reproductive, and respiratory health: a rapid systematic review. Environ. Sci. Technol. 58 (52), 22843–22864.
Chavez-Dominguez, R., Perez-Medina, M., Aguilar-Cazares, D., Galicia-Velasco, M., Meneses-Flores, M., Islas-Vazquez, L., Camarena, A., Lopez-Gonzalez, J.S., 2021. Old and new players of inflammation and their relationship with cancer development. Front. Oncol. 11, 722999.
Chen, H., Chen, H., Nan, S., Liu, H., Chen, L., Yu, L., 2022. Investigation of microplastics in digestion system: effect on surface microstructures and probiotics. Bull. Environ. Contam. Toxicol. 109 (5), 882–892.
Cheng, L., Zhuang, Z., Yin, M., Lu, Y., Liu, S., Zhan, M., Zhao, L., He, Z., Meng, F., Tian, S., Luo, L., 2024. A microenvironment-modulating dressing with proliferative degradants for the healing of diabetic wounds. Nat. Commun. 15 (1), 9786.
Demirelli, E., Tepe, Y., Oğuz, U., Aydın, H., Kodat, M., Tok, D.S., Sönmez, M.G., Öğreden, E., 2024. The first reported values of microplastics in prostate. BMC Urol. 24 (1), 106.
Deng, C., Zhu, J., Fang, Z., Yang, Y., Zhao, Q., Zhang, Z., Jin, Z., Jiang, H., 2024. Identification and analysis of microplastics in para-tumor and tumor of human prostate. EBioMedicine 108, 105360.
Di Chiano, M., Rocchetti, M.T., Spano, G., Russo, P., Allegretta, C., Milior, G., Gadaleta, R.M., Sallustio, F., Pontrelli, P., Gesualdo, L., Avolio, C., Fiocco, D., Gallone, A., 2024. Lactobacilli Cell-Free supernatants modulate inflammation and oxidative stress in human microglia via NRF2-SOD1 signaling. Cell. Mol. Neurobiol. 44 (1), 60.
Edlind, M.P., Hsieh, A.C., 2014. PI3K-AKT-mTOR signaling in prostate cancer progression and androgen deprivation therapy resistance. Asian J. Androl. 16 (3), 378–386.
Fu, X., Han, H., Yang, H., Xu, B., Dai, W., Liu, L., He, T., Du, X., Pei, X., 2024. Nrf2-mediated ferroptosis of spermatogenic cells involved in Male reproductive toxicity induced by polystyrene nanoplastics in mice. J. Zhejiang Univ. Sci. B 25 (4), 307–323.
Gandaglia, G., Leni, R., Bray, F., Fleshner, N., Freedland, S.J., Kibel, A., Stattin, P., Van Poppel, H., La Vecchia, C., 2021. Epidemiology and prevention of prostate cancer. Eur. Urol. Oncol. 4 (6), 877–892.
Goswami, S., Adhikary, S., Bhattacharya, S., Agarwal, R., Ganguly, A., Nanda, S., Rajak, P., 2024. The alarming link between environmental microplastics and health hazards with special emphasis on cancer. Life Sci. 355, 122937.
Hansen, R.S., Biørn, S.H., Birk-Korch, J.B., Sheikh, S.P., Poulsen, M.H., Vinholt, P.J., 2023. Prevalence of prostate cancer in men with haematuria: a systematic review and meta-analysis. BJU Int. 131 (5), 530–539.
He, Y., Yin, R., 2024. The reproductive and transgenerational toxicity of microplastics and nanoplastics: a threat to mammalian fertility in both sexes. J. applied toxicol. JAT 44 (1), 66–85.
Hunt, K., Davies, A., Fraser, A., Burden, C., Howell, A., Buckley, K., Harding, S., Bakhbakhi, D., 2024. Exposure to microplastics and human reproductive outcomes: a systematic review. BJOG Int. J. Obstet. Gynaecol. 131 (5), 675–683.
Jin, Z., Yang, Y., Cao, Y., Wen, Q., Xi, Y., Cheng, J., Zhao, Q., Weng, J., Hong, K., Jiang, H., Hang, J., Zhang, Z., 2023. The gut metabolite 3-hydroxyphenylacetic acid rejuvenates spermatogenic dysfunction in aged mice through GPX4-mediated ferroptosis. Microbiome 11 (1), 212.
Jin, Z.R., Fang, D., Liu, B.H., Cai, J., Tang, W.H., Jiang, H., Xing, G.G., 2021. Roles of CatSper channels in the pathogenesis of asthenozoospermia and the therapeutic effects of acupuncture-like treatment on asthenozoospermia. Theranostics 11 (6), 2822–2844.
Kumar, R., Manna, C., Padha, S., Verma, A., Sharma, P., Dhar, A., Ghosh, A., Bhattacharya, P., 2022. Micro(nano)plastics pollution and human health: how plastics can induce carcinogenesis to humans? Chemosphere 298, 134267.
Li, Y., Liang, R., Zhang, X., Wang, J., Shan, C., Liu, S., Li, L., Zhang, S., 2019. Copper chaperone for superoxide dismutase promotes breast cancer cell proliferation and migration via ROS-Mediated MAPK/ERK signaling. Front. Pharmacol. 10, 356.
Lim, S.L., Ng, C.T., Zou, L., Lu, Y., Chen, J., Bay, B.H., Shen, H.M., Ong, C.N., 2019. Targeted metabolomics reveals differential biological effects of nanoplastics and nanoZnO in human lung cells. Nanotoxicology 13 (8), 1117–1132.
Liu, S., Guo, J., Liu, X., Yang, R., Wang, H., Sun, Y., Chen, B., Dong, R., 2023. Detection of various microplastics in placentas, meconium, infant feces, breastmilk and infant formula: a pilot prospective study. Sci. Total Environ. 854, 158699.
Lu, W., Li, X., Wang, S., Tu, C., Qiu, L., Zhang, H., Zhong, C., Li, S., Liu, Y., Liu, J., Zhou, Y., 2023. New evidence of microplastics in the lower respiratory tract: inhalation through smoking. Environ. Sci. Technol. 57 (23), 8496–8505.

Luo, Z.C., Jin, Z.R., Jiang, Y.F., Wei, T.J., Cao, Y.L., Zhang, Z., Wei, R., Jiang, H., 2023. The protective effects and underlying mechanisms of dapagliflozin on diabetes-induced testicular dysfunction. Asian J. Androl. 25 (3), 331–338.
Perdana, N.R., Mochtar, C.A., Umbas, R., Hamid, A.R., 2016. The risk factors of prostate cancer and its prevention: a literature review. Acta Med. Indones. 48 (3), 228–238.
Prado, Y., Aravena, C., Aravena, D., Eltit, F., Gatica, S., Riedel, C.A., Simon, F., 2023. Small plastics, big inflammatory problems. Adv. Exp. Med. Biol. 1408, 101–127.
Sarapultsev, A., Gusev, E., Komelkova, M., Utepova, I., Luo, S., Hu, D., 2023. JAK-STAT signaling in inflammation and stress-related diseases: implications for therapeutic interventions. Mol. Biomed. 4 (1), 40.
Sekhoacha, M., Riet, K., Motloung, P., Gumenku, L., Adegoke, A., Mashele, S., 2022. Prostate cancer review: genetics, diagnosis, treatment options, and alternative approaches. Molecules 27 (17).
Shi, Z., Lin, J., Wu, Y., Fu, S., Wan, Y., Fang, Y., 2022. Burden of cancer and changing cancer spectrum among older adults in China: trends and projections to 2030. Cancer Epidemiol. 76, 102068.
Shorning, B.Y., Dass, M.S., Smalley, M.J., Pearson, H.B., 2020. The PI3K-AKT-mTOR pathway and prostate cancer: at the crossroads of AR, MAPK, and WNT signaling. Int. J. Mol. Sci. 21 (12).
Sung, H., Ferlay, J., Siegel, R.L., Laversanne, M., Soerjomataram, I., Jemal, A., Bray, F., 2021. Global cancer statistics 2020: GLOBOCAN estimates of incidence and mortality worldwide for 36 cancers in 185 countries. CA Cancer J. clinic. 71 (3), 209–249.
Thompson, R.C., Courtene-Jones, W., Boucher, J., Pahl, S., Raubenheimer, K., Koelmans, A.A., 2024. Twenty years of microplastic pollution research-what have we learned? Science 386 (6720), eadl2746.
Wang, Y., Xu, X., Jiang, G., 2023. Microplastics exposure promotes the proliferation of skin cancer cells but inhibits the growth of normal skin cells by regulating the inflammatory process. Ecotoxicol. Environ. Saf. 267, 115636.
Weber, R.A., Yen, F.S., Nicholson, S.P.V., Alwaseem, H., Bayraktar, E.C., Alam, M., Timson, R.C., La, K., Abu-Remaileh, M., Molina, H., Birsoy, K., 2020. Maintaining iron homeostasis is the key role of lysosomal acidity for cell proliferation. Mol. Cell 77 (3), 645–655.e7.
Wu, H., Liu, Q., Yang, N., Xu, S., 2023. Polystyrene-microplastics and DEHP co-exposure induced DNA damage, cell cycle arrest and necroptosis of ovarian granulosa cells in mice by promoting ROS production. Sci. Total Environ. 871, 161962.
Xiong, Z., Kong, Q., Hua, J., Chen, Q., Wang, D., 2025. Cardiotoxicity of polystyrene nanoplastics and associated mechanism of myocardial cell injury in mice. Ecotoxicol. Environ. Saf. 290, 117712.
Xu, Y., Wu, G., Ma, X., Li, J., Ruan, N., Zhang, Z., Cao, Y., Chen, Y., Zhang, Q., Xia, Q., 2020. Identification of CPT1A as a prognostic biomarker and potential therapeutic target for kidney renal clear cell carcinoma and establishment of a risk signature of CPT1A-Related genes. Int. J. Genom. 2020, 9493256.
Xue, C., Yao, Q., Gu, X., Shi, Q., Yuan, X., Chu, Q., Bao, Z., Lu, J., Li, L., 2023. Evolving cognition of the JAK-STAT signaling pathway: autoimmune disorders and cancer. Signal Transduct. Target. Ther. 8 (1), 204.
Yi, C., Liu, J., Deng, W., Luo, C., Qi, J., Chen, M., Xu, H., 2023. Old age promotes retinal fibrosis in choroidal neovascularization through circulating fibrocytes and profibrotic macrophages. J. Neuroinflamm. 20 (1), 45.
Yong, C.Q.Y., Valiyaveettil, S., Tang, B.L., 2020. Toxicity of microplastics and nanoplastics in mammalian systems. Int. J. Environ. Res. Public Health 17 (5).
Zeng, W., Long, X., Liu, P.S., Xie, X., 2023. The interplay of oncogenic signaling, oxidative stress and ferroptosis in cancer. Int. J. Cancer 153 (5), 918–931.
Zhang, Q., Xu, E.G., Li, J., Chen, Q., Ma, L., Zeng, E.Y., Shi, H., 2020. A review of microplastics in table salt, drinking water, and air: direct human exposure. Environ. Sci. Technol. 54 (7), 3740–3751.
Zhu, L., Kang, Y., Ma, M., Wu, Z., Zhang, L., Hu, R., Xu, Q., Zhu, J., Gu, X., An, L., 2024. Tissue accumulation of microplastics and potential health risks in human. Sci. Total Environ. 915, 170004.